High Power Diode-Seeded Fiber Amplifiers at 2 μm – from Architectures to Applications

Alexander M. Heidt, Zhihong Li, and David J. Richardson

***Abstract*—We review recent advances in the development of high power short- and ultrashort pulsed Thulium-doped fiber amplifier (TDFA) systems seeded by semiconductor laser diodes at wavelengths around 2 μm. The diode-seeding and the master oscillator power amplifier (MOPA) design allow for the construction of extremely versatile laser systems that can operate over wide ranges of peak power, pulse energy and repetition rate in the ultrashort picosecond to the long nanosecond pulsed regimes. We present a record peak power of 130 kW and pulse energy of 5 μJ in picosecond mode, while demonstrating user-defined pulse-shaping capabilities at millijoule pulse energy levels in the nanosecond regime from essentially the same amplifier system. The system architecture as well as important design and power scaling considerations are discussed in detail. Additionally, we highlight recent results in the application of these MOPA systems and their high performance TDFA stages in such diverse application areas as next generation telecommunication networks, mid-infrared supercontinuum generation and mid-infrared gas detection in hollow-core photonic bandgap fibers.**

***Index Terms*—Fiber lasers, Fiber nonlinear optics, Gas detection, Hollow-core fibers, Mid-infrared fiber optics, Semiconductor lasers, Supercontinuum generation, Telecommunications, Thulium-doped fiber amplifiers, Ultrafast optics.**

I. Introduction

Short- and ultrashort pulsed fiber lasers operating at 2 μm wavelength have recently experienced a fast-paced development. The slowing progress in the power scaling of Yb-based fiber systems at 1 μm has shifted the interest of the high power fiber laser community towards Thulium-doped fiber amplifiers (TDFAs) [1, 2]. Working at 2 μm has profoundly beneficial effects for the power scaling potential of fiber lasers, because the mode area of the fundamental guided mode in a fiber increases with the square of the wavelength. This promises up to a 4-fold increase of both nonlinear thresholds and saturation energy, which are favorable conditions for peak power and pulse energy extraction [1, 3]. Consequently, in both the nano- and femtosecond regimes the 1 MW peak power threshold has now been reached or surpassed and further power scaling can be expected to occur rapidly [4, 5].

High peak power pulses at 2 μm wavelength combined with the characteristic advantages of fiber lasers, such as high beam quality, compactness and the potential for maintenance-free operation, are particularly beneficial from an applications point of view and enable, for example, coherent nonlinear frequency conversion further into the mid-infrared waveband, material or medical tissue ablation, and high-intensity physics [3, 6-10]. Table 1 gives an overview of the current maximum peak power levels reported for the different pulse regimes of TDFA systems. Q-switched nanosecond oscillators based on a large-pitch thulium-doped photonic crystal fiber (PCF) rods with 80 μm core diameter have been scaled up to 2.4 mJ pulse energy and 150 kW peak power [11]. Further power scaling is possible in master oscillator power amplifier (MOPA) configurations, and the amplification of 6.5 ns Q-switched pulses to ~1 MW peak power (6.4 mJ pulse energy) has been demonstrated using a 3-stage MOPA system and a similar PCF-rod design in the power amplifier [4]. Femtosecond systems based on chirped pulse amplification in step-index large-mode-area (LMA) fiber with 25 μm core diameter have achieved 35 MW peak power with a pulse energy of 37 μJ and 910 fs pulse duration after external compression [5]. Further scaling to 156 μJ pulse energy was demonstrated, although the pulses were not completely compressed in this instance [12].

In the quest for scaling the power of pulsed fiber laser systems at 2 μm, the picosecond regime seems to have been somewhat overlooked. Prior to the work reviewed in this paper, peak powers of the order of only 10 kW were reported [13, 14] falling significantly short of the performance levels achieved in other pulse regimes. This can be attributed mainly to the lack of an attractive seed source, as the (spectrally filtered) mode-locked oscillators used in these early reports are not the most convenient choice. In the 1 μm wavelength region, gain-switched semiconductor diode lasers have proven highly successful and versatile sources of picosecond pulses, and when amplified in MOPA systems based on Yb-doped fibers have delivered average power levels of several hundred Watts and peak powers up to 270 kW [15-18]. Additionally,

This work was supported by the EU 7th Framework Program under grant agreement 258033 (MODE-GAP) and by the UK EPSRC through grant EP/I01196X/1 (HYPERHIGHWAY) and EP/H02607X/1 (Centre for Innovative Manufacturing in Photonics). D.J.R. gratefully acknowledges support from the Royal Society through a Wolfson Research Merit Award. A.M.H. is supported by the EU People Programme (Marie Curie Actions) under grant agreement 300859 (ADMIRATION). Z.L. thanks the China Scholarship Council for financial support.

TABLE I
CURRENT PEAK POWER LEVELS OF THULIUM-DOPED FIBER AMPLIFIER SYSTEMS IN DIFFERENT PULSE REGIMES

	Nano-second	Pico-second	Femto-second
Peak Power	1 MW (6.4 mJ, 6.6 ns)	Prior: ~10 kW [12, 13] Here: 130 kW (5 µJ, 38 ps)	35 MW (37 µJ, 910 fs) [b]
Fiber Core Diameter [a]	80 µm	25 µm	25 µm
Fiber Type [a]	PCF rod	Step-index LMA	Step-index LMA
Seed Source	Q-switched fiber laser	Gain-switched laser diode	Mode-locked fiber laser
Reference	[4]	-	[5]

[a]refers to the largest gain fiber used in the MOPA system. [b]chirped pulse amplification, refers to pulse parameters after external compression.

such diode-seeded laser systems have enabled pulse-shaping in the pico- and nanosecond regime for the compensation of gain saturation effects or the generation of user-defined pulse shapes in material processing [19, 20]. In the 2 µm wavelength region, however, these concepts have yet to be properly exploited.

In this paper we review our recent advances in the development and application of high-performance, low-noise TDFAs and MOPA systems seeded by semiconductor laser diodes at 2 µm. By gain-switching of the seed diode we obtain compact, practical and reliable fiber sources of picosecond pulses with record peak powers up to 130 kW (5 µJ energy, 38 ps duration) that can provide many of the proven advantages of femtosecond systems, but with great benefits of in terms of system cost and complexity. Specifically, the dispersion management employed in high-power femtosecond systems can be avoided, while the significantly shorter pulse duration compared to nanosecond Q-switched systems is attractive for many uses, e.g. for nonlinear frequency conversion. Note that we do not employ rod-type fibers in our amplifiers in order to maintain compactness, and as a consequence fall short of recent record peak power demonstrations at nanosecond durations. Nevertheless, these results represent an order-of-magnitude increase of peak power and pulse energy compared to picosecond systems reported prior to this work and are achieved using a highly practical system configuration.

We further demonstrate that the diode-seeding approach allows for the construction of agile laser systems that can provide high pulse energy, high peak power, and widely adjustable pulse duration and repetition rates and that hence are suitable for a wide range of applications while maintaining overall simple system architectures. This versatility is simply achieved by controlling the electrical drive current of the seed diode, which allows us to generate ultrashort high peak power picosecond pulses from the same laser system that we use for the generation of user-defined nanosecond pulse shapes at millijoule energy levels. We further highlight the flexibility and functionality of the MOPA systems and TDFA sub-components by reviewing our latest results in the implementation of these devices in such diverse application areas as next generation telecommunication networks, mid-infrared (mid-IR) supercontinuum generation, and mid-IR gas detection in hollow-core fibers.

The structure of the paper is organized as follows. Section II gives a detailed description of the architectures of the 2 µm diode-seeded MOPA systems used in this work and associated components, and discusses important design and power scaling considerations. Section III details the MOPA performance in high peak power picosecond and high pulse energy nanosecond operation, and presents the pulse shaping capabilities of the system. Finally, application examples are discussed in section IV.

II. SYSTEM ARCHITECTURES

A. Overview

We consider two implementations of short- and ultrashort-pulsed TDFA systems in a MOPA configuration, denoted A and B in Fig. 1. Both systems are extremely versatile and can operate over a wide range of repetition rates in the picosecond- as well as nanosecond-pulsed regimes, but address different aspects in terms of system simplicity and pulse energy / peak power scaling. As a common feature they are both seeded by a fiber-pigtailed laser diode operating in the vicinity of 2 µm (master oscillator), followed by a 3-stage TDFA system. The seed is a discrete-mode InGaAs/InP laser diode (Eblana Photonics), which is a ridge waveguide Fabry-Perot (FP) diode constrained to lase in a single longitudinal mode of the FP cavity by appropriate super-structuring of the chip with multiple quantum wells [21]. Here we use seed-diodes with operating wavelengths of 2008 nm and 1952 nm, but a range of diodes with central wavelengths of 1700 – 2050 nm have now been developed, making it possible to access user-defined laser wavelengths anywhere in the TDFA amplification window with only minor changes in the system configuration.

The seed-diodes typically emit peak powers only of the order of a few milliwatts in pulsed operation. The subsequent TDFA amplifier chain is therefore required to deliver a total gain of up to 70 dB in order to achieve the targeted peak power and pulse energy levels. The achievement of such high gain values requires efficient and low-noise pre-amplifiers, and the management of amplified spontaneous emission (ASE) as well as the control of nonlinearities become critical issues. The main difference between configurations A and B in Fig. 1 is the way these critical issues are addressed and consequently they differ in their practical operating conditions.

We first review our recent advances in the development of high performance low noise pre-amplifiers in section II.B, before discussing design details and power scaling considerations for the complete amplifier chains in section II.C.

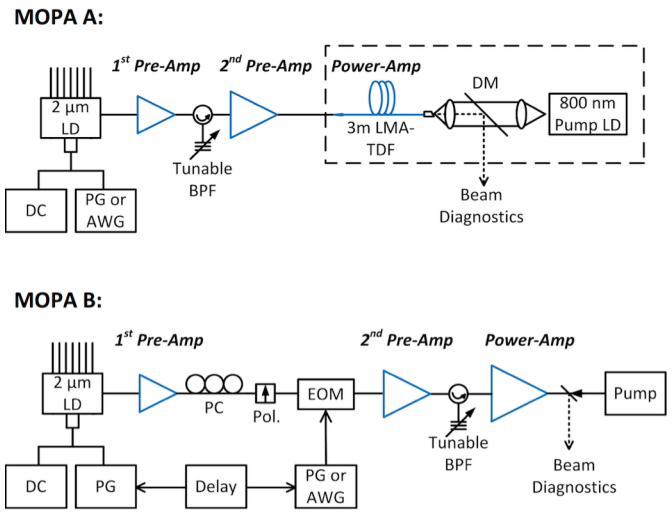

Fig. 1. Schematic experimental setup of the two MOPA systems constructed. LD: laser diode; BPF: band-pass filter; LMA-TDF: large-mode-area thulium-doped fiber; DM: dichroic mirror; PG: pulse generator; AWG: arbitrary waveform generator; PC: polarization controller; Pol: polarizer; EOM: electro-optic modulator.

B. High performance low-noise pre-amplifiers

Fig. 2 exemplary illustrates the design of our single-mode core-pumped pre-amplifiers and the conceptual idea that allows us to optimize their performance in different wavelength regions. In Fig. 2 (a), the schematic setup of two amplifier configurations is illustrated that were developed to provide high gain, low-noise amplification at short and long wavebands, respectively [22]. The first design, called TDFA-C, consists of a 12 m long commercially available TDF (OFS TmDF200) with 6.2 µm mode field diameter (MFD) and

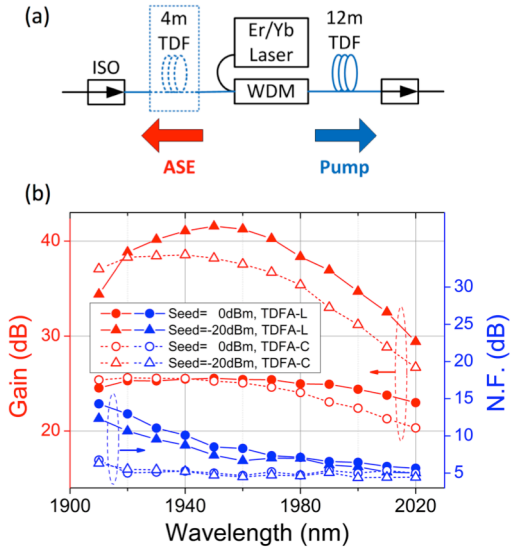

Fig. 2. (a) Design of the single-mode core-pumped pre-amplifiers. The optional 4 m of Thulium-doped fiber (TDF), pumped by backward-travelling amplified spontaneous emission (ASE), optimizes the gain for long operating wavelengths. (b) Gain and noise figure (N.F.) performance of the amplifier for small (-20 dBm) and saturated (0 dBm) CW input signals. TDFA-L denotes the design including the optional 4 m TDF, TDFA-C without this fiber [22].

20 dB/m core absorption, forward pumped by an Er/Yb co-doped fiber laser at 1565 nm. Pump and signal wavelengths are combined using a WDM coupler, and isolators at both ends prevent parasitic lasing. The second design (TDFA-L) includes an additional 4 m TDF inserted between the input isolator and WDM coupler. This additional piece of fiber is indirectly pumped by the backward-travelling ASE generated from the directly pumped 12 m TDF section.

Fig. 2 shows the wavelength-resolved gain performances and external noise figures (NF) of both designs for small (-20 dBm) and saturated (0 dBm) continuous wave (CW) input signals at a fixed pump power of 31 dBm. The introduction of the additional indirectly pumped section of gain fiber in TDFA-L has two distinct effects. Firstly, the amplifier gain is significantly enhanced for long wavelengths (3-4 dB for $\lambda \geq 1950$ nm), reaching up to 41 dB at 1950 nm, and the saturated gain flatness is improved. This can be attributed to the reabsorption of the otherwise lost backward-travelling ASE, which enhances the amplifier efficiency, and the overall longer length of gain fiber, which shifts the gain peak towards longer wavelengths due to the quasi three-level system behaviour of Thulium-doped silica at room-temperature. Secondly, the gain enhancement at long wavelengths is achieved without paying a significant penalty in terms of NF, which remains at 5 - 7 dB. However, the NF increases at shorter wavelengths due to increased initial absorption of the input signal. Note that the passive components used in these measurements have a combined insertion loss of 2.5 dB, which is the main limiting factor of NF performance. We could recently demonstrate NFs as low as 4.5 dB using improved isolators and WDM couplers [23] and expect this value to drop further towards the 3 dB quantum noise limit as the increased interest in this wavelength region will drive the development of low-loss commercial components.

TDFAs optimized in this way are well suited for high gain, low-noise pre-amplification in high power systems, and saturated output powers of well beyond 1 W with 50% slope efficiency and excellent optical signal-to-noise ratio (OSNR) for 1 mW of input signal could be demonstrated [22]. By choosing the correct lengths of directly- and ASE-pumped active fiber segments, the design can be adapted to operate anywhere in the Thulium amplification bandwidth, and devices covering the 1720 – 2050 nm window have recently been presented [23].

These TDFA designs also attract growing interest for the application as high performance amplifiers in potential future telecommunication networks operating at wavelengths around 2 µm. The TDFAs are analogous in implementation and function to the current Erbium-doped fiber amplifiers (EDFAs), but capable of operating over a far more extended bandwidth in this new waveband of interest and therefore provide significant potential for enhanced data transmission capacities. This application area will be discussed in more detail in section IV.A.

C. MOPA design and power scaling considerations

In this section we detail the experimental setup of the high power MOPA systems in Fig. 1 and discuss fundamental design and power scaling considerations.

In MOPA A, the seed-diode is driven directly by a fast electrical pulse generator (PG) or arbitrary waveform generator (AWG). The details of the driving electronics depend on the desired pulse width and pulse shaping functionality and will be discussed in section III. The first pre-amplifier is configured in the TDFA-L layout discussed in section II.B. A subsequent tunable bandpass filter (BPF) removes excess out-of-band ASE. In its first generation this filter consisted of two fiber Bragg gratings in series [24], but was later replaced by a more versatile fiber-pigtailed grating-based filter with a -3 dB passband of 3 nm and a tuning range covering the entire Thulium amplification bandwidth [25]. In order to minimize nonlinearities, the TDFA-C configuration is used for the second pre-amplifier and the commercial active fiber is replaced by an in-house drawn TDF with larger core diameter (8.3 µm) and higher doping concentration. This allows us to reduce the active fiber length to 2.2 m. The output of the second pre-amplifier is taper-spliced to a 3 m-long large-mode area double-clad TDF with a 25 µm diameter, 0.09 NA core and 250 µm cladding (Nufern). The free end of the fiber is terminated with an angle-polished end-cap avoiding signal feedback and allowing beam expansion and reduction of the peak intensity at the glass/air interface. The power amplifier is free-space cladding-pumped in a counter propagating configuration with up to 60 W of coupled pump power provided by a fiber-pigtailed pump diode at 800 nm (Jenoptik). The output is near-diffraction-limited with a measured beam quality factor $M^2 < 1.3$.

Note that we do not pump at the Thulium:silica absorption maximum of 793 nm, but slightly offset at the wings of the absorption peak between 800 – 805 nm. The lower pump absorption allows us to achieve population inversion over a longer length of fiber, which in turn pushes the gain maximum to longer wavelengths. This maximizes the gain at our operating wavelengths and has the additional advantage that more established and cost-effective 808 nm pump diodes can be employed, which are routinely used for Nd:YAG bulk solid-state laser systems and can be temperature tuned to shorter wavelengths.

In this amplifier system we employ a simple and passive approach to ASE management using only a single BPF after the first pre-amplifier. This results in high system simplicity and works well for high average powers and pulse repetition rates when all amplifiers are seeded well into their saturation regime and ASE build-up is limited. In this case, most of the total gain is provided by the pre-amplifiers, only the final 10 – 15 dB are contributed by the power amplifier. For low repetition rates and high pulse energies / peak powers, however, it would be advantageous to limit the power in the pre-amplifiers and redistribute the gain towards the power amplifier stage where the large mode-field diameter increases the threshold for the onset of nonlinearities.

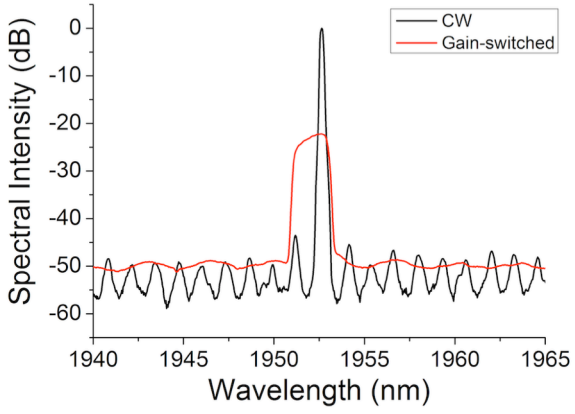

Fig. 3. Exemplary spectrum of the seed diode spectrum in CW and gain-switched mode, centered at a wavelength of 1952 nm.

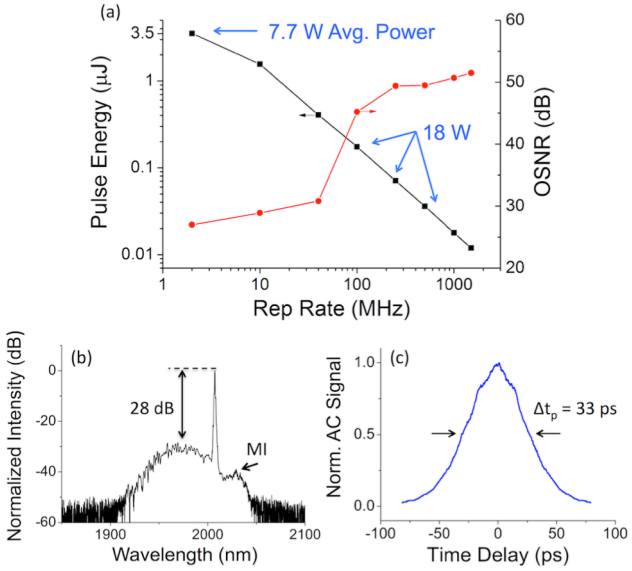

Fig. 4. Summary of MOPA A performance in the picosecond regime. (a) Pulse energy and optical signal-to-noise ratio (OSNR) as a function of the repetition rate. Indications of average power at low and high repetition rates are also given. (b) Spectrum and (c) autocorrelation trace recorded at 2 MHz repetition rate and 3.5 µJ pulse energy [24].

This redistribution of gain is achieved with MOPA B in Fig. 1. It uses the same building blocks as MOPA A, but arranged in a different manner and includes an electro-optic modulator (EOM; Photline Technologies) introducing additional filtering and pulse shaping capabilities to the system. The EOM is inserted after the first pre-amplifier and acts as a time-gate, passing (and if desired shaping) the amplified signal pulses, but blocking the in-band ASE that builds up temporally in between two subsequent pulses at low repetition rates. Since the EOM is polarization sensitive, it requires a polarization controller and a fast-axis blocking polarizer at the input. Additionally, the BPF filters out-of-band ASE before injection into the power amplifier. This effective ASE suppression enables us to run all amplifiers with small-signal inputs and to extract up to 30 dB gain from the final power amplifier stage. Consequently, we generally achieve significantly better optical signal-to-noise ratios (OSNR) and higher nonlinear thresholds with MOPA B, enabling better pulse energy and peak power scaling as compared to MOPA A through the ability to operate at lower repetition rates. However, this comes at the cost of increased system complexity as the EOM requires further driving electronics and synchronization to the diode pulses.

III. Performance in Different Pulse Regimes

A. *Picosecond regime: gain-switching*

We generate picosecond pulses directly at 2 µm wavelengths by gain-switching the seed laser diode using short rectangular electrical pulses of 350 ps duration and 5 V amplitude supplied by a pulse generator. The resulting optical pulse widths are generally shorter than the electrical excitation pulses and are determined by the carrier-photon interaction dynamics [26, 27]. A below-threshold DC voltage is applied to optimize the pulse parameters. In this way we obtain pulse durations in the range of 40 – 50 ps from the laser diodes used in this work.

The typical spectral response of the latest generation of seed diodes in CW and gain-switched operation is shown in Fig. 3. In CW mode, the diode exhibits single longitudinal mode operation with a spectral bandwidth of approximately 600 kHz [21]. The side modes of the FP cavity are suppressed to the -45 dB level relative to the spectral peak and the mode spacing is about 1.5 nm. In gain-switched operation the spectral bandwidth broadens to a -3 dB width of 1.6 nm. Note that in earlier generations of seed diodes used in MOPA A, significant excitation of the FP side modes was observed that required removal by spectral filtering, resulting in a much narrower spectral bandwidth [24].

The performance of MOPA A, which operates at a central wavelength of 2008 nm, was investigated in detail in [24] and is summarized in Fig. 3. A maximum pulse energy of 3.5 µJ can be extracted from the system at 2 MHz repetition rate and 7.7 W of average output power. Through the interplay of nonlinear self-phase modulation (SPM) and the anomalous dispersion of the active fiber we observe a temporal compression of the pulses from 45 ps measured after the pre-amplifiers to 33 ps at the output of the power amplifier. This corresponds to a peak power of ~ 100 kW.

The amplifier system can be operated with variable repetition rates in the range 2 MHz – 1.5 GHz. At low repetition rates, the maximum peak power is limited by the build-up of ASE with a peak at 1970 nm as well as by the onset of modulation instability (MI), which creates spectral side lobes through the amplification of random noise via phase-matched four-wave mixing processes [28]. The long-wavelength MI peak at 2030 nm is readily visible in Fig. 3 (b), while the corresponding symmetrical peak at the short wavelength side of the signal, expected around 1990 nm, is concealed by ASE. At higher repetition rate, the system performance is pump power limited, leading to a linear reduction of pulse energy with increasing repetition rate at a constant average power of 18 W, as shown in Fig. 3 (a). The OSNR increases from 28 dB at 2 MHz to over 50 dB at 1.5 GHz due to the improved seeding of all amplifier stages.

The stability and reliability of the pulse generation and amplification process is an important feature for many applications. We measured a temporal jitter of < 2 ps over a 60 s period, limited by the bandwidth of our detection equipment. Earlier experiments at 1550 nm have highlighted

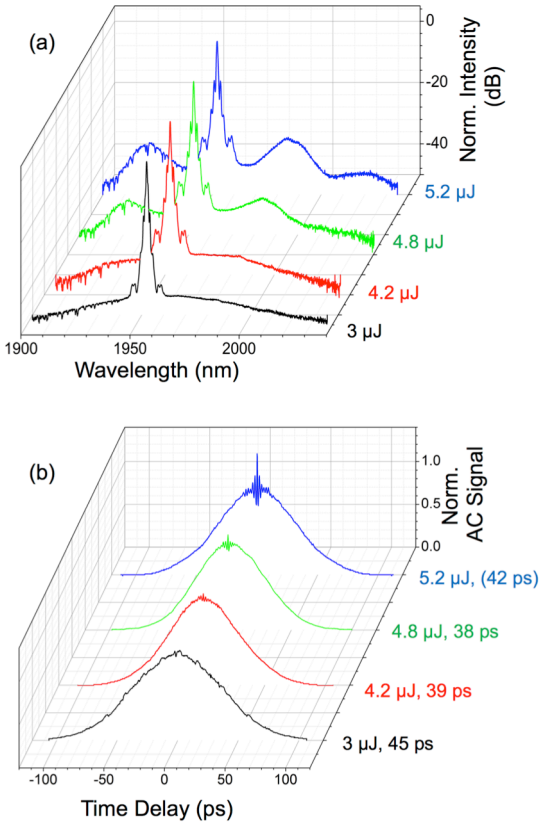

Fig. 5. Performance of MOPA B in high pulse energy picosecond operation. (a) Evolution of the spectrum as a function of the pulse energy, and (b) corresponding autocorrelation traces. The onset of modulation instability (MI) can clearly be identified in both cases.

the exceptional inherent temporal stability of gain-switched discrete-mode diode lasers and demonstrated a jitter as low as 450 fs [29]. We expect a similar performance in this implementation at 2 µm. In subsequent experiments we have operated the system over many weeks for several hours per day and found its operation extremely reliable and repeatable. No performance degradation or needs for readjustments were observed so far.

In order to investigate the possibilities for further power scaling we use MOPA B, which includes an EOM for additional in-band ASE filtering. This allows us to operate at lower repetition rates and redirect gain from the pre-amplifiers to the power amplifier, which reduces the effective nonlinearity of the system. The EOM is driven by an additional pulse generator and synchronized to the arrival of the diode pulses using a time gate width of 2.4 ns.

Fig. 4 summarizes the high pulse energy performance of MOPA B, operated at a central wavelength of 1952 nm and 1 MHz repetition rate. The spectra in Fig. 4 (a) illustrate that ASE is effectively suppressed and the OSNR is consistently above 40 dB. The clean spectra allow us to observe the nonlinear behavior of the system in more detail. As the pulse energy is increased from 3 µJ to 5.2 µJ, two distinct nonlinear effects can be identified. Firstly, the central spectral peak broadens due to SPM, which amplifies additional longitudinal modes from the seed diode that become visible as fine

structure around the central peak (compare Fig. 3). In the time domain, this is accompanied by the nonlinear compression of the pulses from 49 ps measured after the pre-amplifier to 38 ps at 4.8 µJ. Secondly, the MI threshold is reached at 4.8 µJ pulse energy when side-peaks appear at 1920 and 1985 nm. In the time domain, the presence of these side peaks results in a temporal beating superimposed on the peak of the pulse envelope, which is clearly visible in the autocorrelation trace. At 5.2 µJ energy, both MI spectral peaks and the temporal beating amplitude have substantially increased, which makes the extraction of the pulse width from the autocorrelation trace unreliable as the pulse shape might have changed. Hence the measured 42 ps are set in brackets in Fig. 5 (b); instead we would expect a continued temporal compression.

In summary, we can extract up to 5 µJ pulse energy and a pulse width of about 38 ps from MOPA B before MI becomes significant, corresponding to a peak power of ~ 130 kW. Note that the onset of MI in the amplifier at higher energies might be beneficial for some applications, e.g. for mid-IR supercontinuum generation, where MI-initiated soliton fission plays an important role [30]. The modest 30% peak power increase in comparison to MOPA A lets us conclude that the system performance is mainly limited by nonlinearity in the final amplifier stage. Fibers with larger core diameters, e.g. rod-type fibers, will therefore be required to achieve further pulse energy and peak power scaling in the picosecond regime.

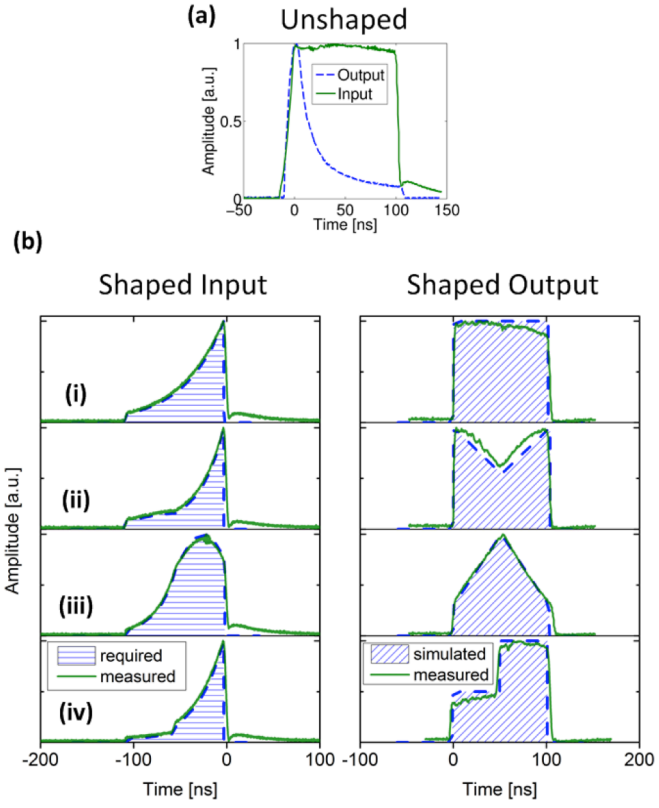

Fig. 6. Compensation of gain saturation and user-defined pulse shaping using direct modulation of the seed diode in MOPA A. The output pulse energy is 0.5 mJ in all cases. The unshaped pulse on top shows the typical signature of reshaping due to gain saturation with preferential amplification of the leading edge. The shaped results (i) – (iv) show a selection of user-defined output pulses and the corresponding input shapes required to generate them [31].

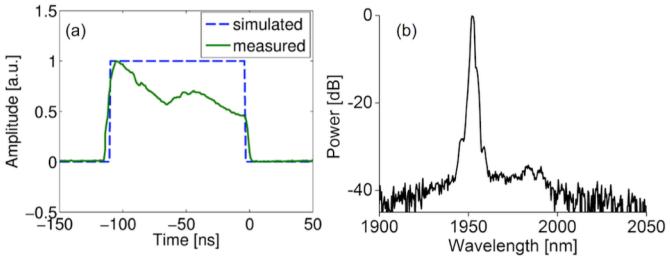

Fig. 7. Generation of 1.0 mJ pulses using the EOM as a pulse shaping device in MOPA B. The pulse shaping in (a) is not perfectly matched to the required profile due to the limited EOM dynamic range, however it prevents the onset of SBS occurring at 0.25 mJ without shaping. The spectrum in (b) is free of ASE and nonlinear signatures, indicating further power scaling potential [31].

B. Nanosecond regime: user-defined pulse-shaping

The design of our MOPA systems allows us to access a wide range of pulse durations simply by controlling the drive current to the seed diode. Here we exemplary highlight this versatility by demonstrating the amplification of 100 ns pulses to energies of up to 1 mJ with the same amplifier configurations that we used previously for the picosecond regime. Additionally, we are able to control the shape of the seed pulses either by direct modulation of the seed diode, or with the EOM, in order to compensate the effects of gain saturation in the amplifiers and access user-defined pulse shapes at the system output [31].

Initially we use MOPA A and drive the seed diode with a computer controlled AWG connected to an RF amplifier that delivers a maximum voltage of 7 V. Again, a below-threshold DC voltage is applied for fine control over the pulse parameters. The seed rise time is set to a minimum of 16 ns in order to avoid spiky relaxation oscillations at the pulse front.

Fig. 6 (a) compares the original seed pulse and the amplifier output using the squarest available pulse from the seed diode, amplified to 0.5 mJ energy (12.5 W at 25 kHz). Clearly, the pulse undergoes substantial gain reshaping, which is a common phenomenon in fiber amplifiers caused by the modest saturation energies of the gain fibers [32, 33]. The pulse front experiences preferential gain, resulting in a reduced pulse width and higher peak power. Since this effect increases the sensitivity to nonlinearities, it is particularly important to compensate for gain saturation effects if high pulse energies are to be extracted from the amplifier. In our system gain saturation occurs predominantly in the power amplifier, there is only negligible reshaping in the pre-amplifiers.

An analytical description of gain saturation shows that the input and output pulse shapes of an amplifier are connected by a simple transfer function [32]. This function essentially only depends on two system parameters, namely small-signal gain and saturation energy, which can easily be extracted from a fit to the amplifier response for a square test pulse. It is then possible to obtain any desired arbitrarily shaped output pulse by applying the inverse transfer function and finding the required input pulse shape. This method is now routinely used

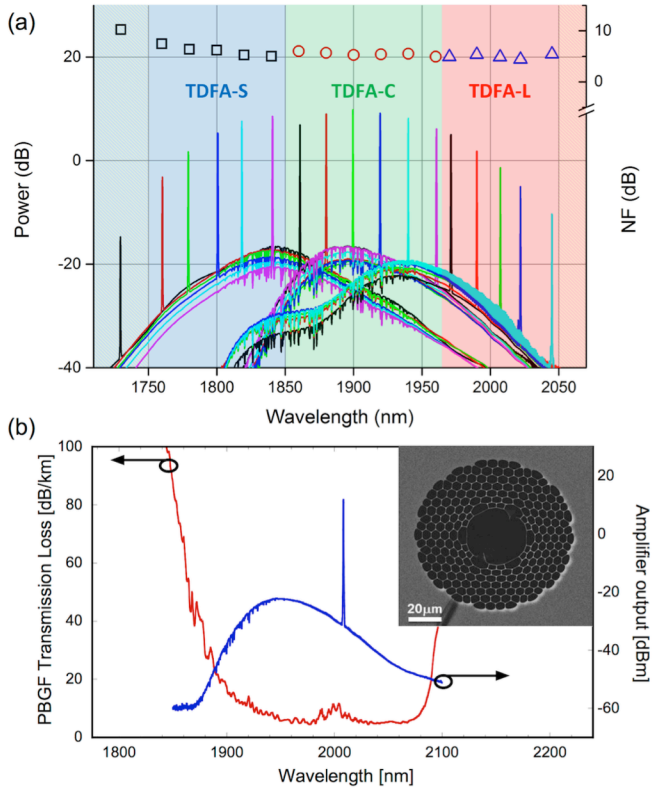

Fig. 8. Application of TDFAs in optical fiber communications at 2 µm. (a) Amplified spectra and corresponding noise figure (NF) of diode-pumped TDFAs based on the design of the pre-amplifiers discussed in section II.B. By combining TDFA-S/C/L optimized for short, central, and long waveband operation, respectively, high-gain low-noise amplification covering the entire Thulium gain bandwidth in the range 1720 – 2050 nm can be achieved. (b) Cross section and loss spectrum of the HC-PBGF used in recent 2 µm data transmission experiments, overlapped with the output of TDFA-L showing the amplified data channel. The transmission bandwidth of the fiber matches well with the gain bandwidth of the TDFA [47].

at 1 µm and 1.5 µm [19, 34, 35], but has never been demonstrated before at 2 µm.

Fig. 6 (b) shows the calculated input pulses required to obtain 0.5 mJ output pulses with a selection of user-defined shapes and compares them with the experimental measurements, obtained by direct modulation of the seed diode using the AWG. There is an excellent agreement between targeted pulse shapes and measured profiles. Further energy scaling beyond 0.5 mJ in MOPA A is limited by the low peak power available directly from the diode (~ 5 mW). For the compensation of gain saturation at higher pulse energy, strong shaping with a high dynamic range is required, which reduces the seed average power to impractically low levels with our current diodes.

MOPA B allows energy scaling to 1.0 mJ and beyond by making use of the EOM as a pulse shaping device. In this case the seed diode is set to emit square pulses of 300 ns duration. These initial pulses are then amplified in the first pre-amplifier without distortion, from which the EOM, directly driven by the AWG carves 100 ns pulses with the required pulse shape. This ensures sufficient seeding of the subsequent amplifiers and enables us to operate at a lower repetition rate of 12.5 kHz.

Fig. 7 shows the output pulse shape and spectrum at 1.0 mJ pulse energy. The extreme gain reshaping occurring at these high energies is clearly compensated, although the profile does not exactly match the desired square shape due to the limited extinction ratio of the EOM (20 – 23 dB at 1950 nm). However, without shaping we observe the onset of stimulated Brillouin scattering (SBS) already at 0.25 mJ in this system, caused by the narrow linewidth of the seed in long pulse operation in combination with the high peak power of the amplified unshaped pulses. This clearly highlights the importance and effectiveness of the pulse shaping approach. The spectrum in Fig. 7 (b) is free of ASE or nonlinear signatures, confirming the potential for further energy scaling using EOMs with higher extinction ratio or acousto-optic modulators.

IV. Applications

A. *Next-generation telecommunication networks*

The ever-increasing volume of internet traffic drives today's telecom networks rapidly towards their capacity limits [36-39]. Traditionally, research efforts in long-haul telecom networks have been focused on the 1.55 µm wavelength region defined by the amplification bandwidth of the EDFA and the low-loss transmission window of single-mode silica fiber (SMF). More recently, however, radical approaches in more exotic fiber types are actively being pursued to increase the transmission capacity per fiber, decrease fiber loss and nonlinearity and reduce signal latency [40-42], which may eventually justify a shift away from the traditional operating wavelengths.

TDFAs exhibit a gain bandwidth of about 30 THz, which is more than twice as large as the EDFA bandwidth (~12 THz for current C + L band) and is the broadest of all rare-earth doped fiber amplifiers [3]. Hence they represent an attractive route towards significantly enhanced transmission bandwidths by offering the potential to amplify a large number of additional wavelength-division multiplexed (WDM) communication channels. TDFAs based on the design principles discussed in section II.B (Fig. 2) have now been extensively characterized in an optical communications context and were found to be a viable alternative to modern EDFAs [22]. Since diode-pumped versions have been developed [23], where the fiber laser pump source in Fig. 2 (a) is replaced by in-band pumping 1550 nm laser diodes, TDFAs have now truly reached a similar level of compactness, reliability and efficiency as current Erbium-based systems. In Fig. 8 (a), high gain low noise amplification over the entire Thulium gain bandwidth of more than 300 nm from 1720 – 2050 nm is demonstrated by combining three of these compact devices optimized for short, central, and long waveband operation, respectively. Based on these TDFA designs, a compact diode-pumped all-fiber thulium-doped laser with more than 250 nm of continuous tuning range could also be realized [25]. This recent maturation of the TDFA certainly confirms the practicality of 2 µm optical fiber communications from an amplifier perspective.

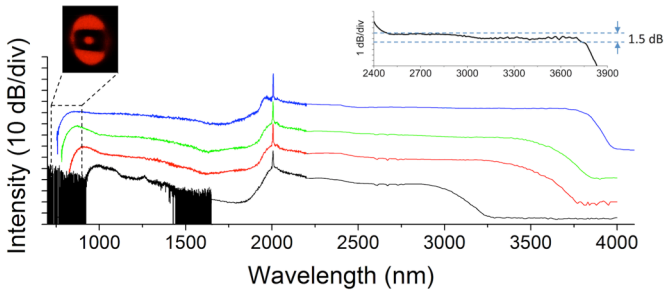

Fig. 9. Supercontinuum generation using high peak power picosecond pulses from MOPA A directly coupled into 7 m of highly nonlinear ZBLAN fiber. The spectra were generated using pulse energies of 185 nJ (black), 300 nJ (red), 600 nJ (green), and 1100 nJ (blue); offset for clarity. The insets show the exceptional flatness of the mid-IR part of the broadest spectrum, and the far-field multi-mode beam profile of the ZBLAN output at visible wavelengths. The fiber is single-moded for wavelengths above ~ 2800 nm [69].

The development of low loss transmission fibers will however be the key factor determining whether 2 µm communications will ultimately outperform current 1.55 µm systems. Hollow-core photonic bandgap fibers (HC-PBGF) are promising candidates for such a new generation of transmission fibers due to their ultralow nonlinearity and a more than 30 % faster transmission speed compared to conventional solid fibers [41]. These properties originate from the light guidance in their hollow core with minimal overlap (as low as 0.1 %) with the surrounding silica glass structure [43]. This low overlap factor is also responsible for reducing infrared absorption and shifting their minimum loss to wavelengths around 2 µm – conveniently coinciding with TDFA territory [44, 45].

In a recent proof-of-principle experiment, the error-free transmission of an amplified 8 Gbit/s data channel at 2 µm over 290 m of HC-PBGF was demonstrated for the first time [46, 47]. The fiber's more than 150 nm wide transmission window with minimum loss of 4.5 dB/km overlaps well with the amplification bandwidth of TDFA-L discussed in II.B, as shown in the comparison in Fig. 8 (b). WDM transmission of 4 data channels was later reported using the same fiber and amplifier [48]. Interestingly, many of the building blocks of the MOPA systems described in this paper were also used for these transmission experiments, clearly showing the beneficial interdependence of high power fiber laser and telecom system research.

Currently, strong efforts are being directed towards determining the intrinsic loss limits of HC-PBGF and fabricating fibers with broader transmission windows and loss values closer to those of conventional SMFs [49]. However, it is now clearly established that HC-PBGFs can meet the challenging requirements of modern data modulation formats and 30.7 Tbit/s (96x320Gbit/s) dual polarization (DP)-32QAM coherently detected transmission over HC-PBGF at 1.55 µm has been demonstrated [50]. They also offer the possibility to implement novel capacity-enhancing techniques such as space division multiplexing (SDM) [40], as impressively shown by a record capacity of 73.7 Gbit/s through a combination of dense WDM and SDM using the three lowest order modes of a HC-PBGF [51]. The development of low-loss splicing techniques using standard equipment further confirms the practicality of these fibers [52, 53]. Certainly, the combination of TDFAs and HC-PBGFs operating at 2 µm is one of the most radical approaches for next-generation telecom networks, but also one of the most exciting ones for high power fiber laser research, as the development of new laser diodes, low-loss components, high-performance amplifiers and low-nonlinearity beam delivery fibers can be expected at this emerging waveband.

B. Mid-IR supercontinuum generation

The high peak powers and short pulse durations emitted by our MOPA systems in gain-switched picosecond mode are ideally suited for nonlinear frequency conversion further towards mid-IR wavelengths. Supercontinuum generation (SCG) in nonsilica fibers made from nonlinear mid-IR transparent glasses (e.g. fluoride, tellurite, or chalcogenide) is a promising approach to meet the increasing demands for broadband, high-brightness mid-IR radiation in various application areas, e.g. molecular fingerprinting, chemical sensing or gas detection (see section IV.C) [54, 55]. Of all possible materials, heavy metal fluoride glass (ZBLAN) is currently the most attractive choice for constructing practical SCG sources due to its high transparency up to ~ 4.5 µm wavelength, the maturity of the fiber fabrication technology and the commercial availability of highly nonlinear ZBLAN fibers with the required small core diameters. Consequently, SCG in this fiber type has been demonstrated with numerous pumping schemes, predominantly using either femtosecond or nanosecond pulse durations [56-62].

From the perspectives of compactness, reliability, versatility and cost-efficiency, semiconductor laser diodes as master oscillators coupled with fiber amplifiers are the ideal choice of pump system for SCG. They offer a significant control over the properties of the generated SC through their capability to deliver wide ranges of adjustable pump pulse parameters, which has contributed to their scientific and commercial success in the near-IR and visible wavelength regions [63-66].

ZBLAN fibers typically have zero-dispersion wavelengths (ZDWs) between 1.65 – 1.9 µm. Pumping at wavelengths longer than the ZDW in the anomalous dispersion region is advantageous for efficient SCG, and 2 µm pumping in particular leads to an optimization of both bandwidth and conversion efficiency [67]. Prior to this work, however, diode-pumped mid-IR SCG sources had to be based on 1550 nm seed-diodes and therefore had to rely on either nonlinear methods or the use of intermediate pulse-pumped TDF laser cavities to convert to longer pumping wavelengths [55, 56, 68]. Using the MOPA systems presented here, it is now possible to implement the direct picosecond diode-pumping of ZBLAN fibers at 2 µm, which represents a significant improvement in terms of system simplicity, reliability, and stability compared to previous diode-pumped mid-IR sources [69].

Fig. 9 shows the resulting SC spectra when various pulse energies emitted by MOPA A are directly coupled into a 7 m

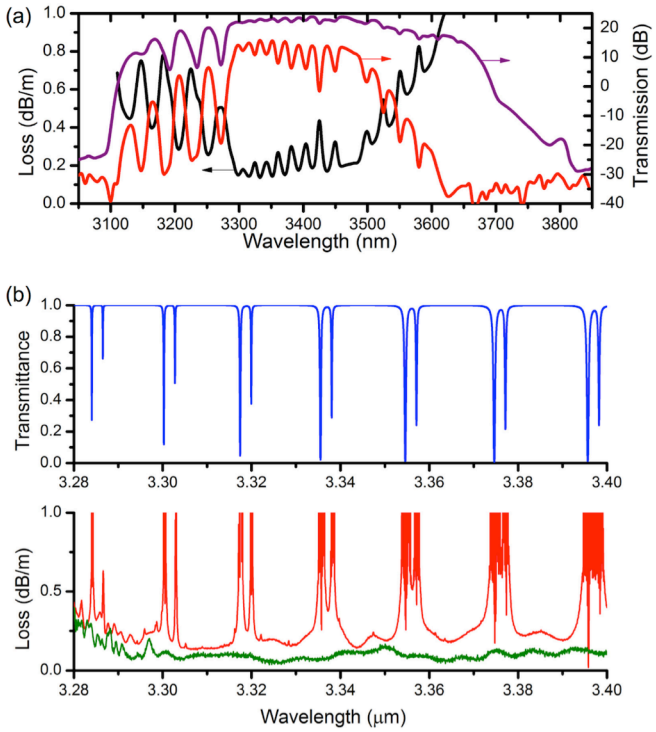

Fig. 10. Low-loss, wide bandwidth mid-IR guidance in silica-based HC-PBGF. (a) Transmission through 5 m (purple), 58 m (red), and corresponding attenuation calculated from cutback measurement (black). (b) HCl gas absorption spectrum from HITRAN database (top) and high resolution (0.2 nm) attenuation measurements before and after purging the fiber with argon. The peaks in the attenuation spectrum can clearly be attributed to the presence of HCl gas outgassing from the raw materials used in fiber fabrication. All spectra were taken using the mid-IR SCG source described in IV.B [80].

long commercial ZBLAN fiber (Thorlabs, 9 μm core diameter, 0.25 NA). The maximum spectral bandwidth of more than two octaves spanning from 750 – 4000 nm is reached for 1.1 μJ pump pulses. Further broadening was limited by the attenuation of the particular fiber in use. The spectra exhibit a remarkable flatness in the mid-IR with a power variation as low as 1.5 dB over a 1300 nm wide spectral range from 2450 – 3750 nm, as shown in the inset of Fig. 9.

The total SC average power is up to 1.1 W at 1 MHz repetition rate, with more than 21% (235 mW) at wavelengths above 2500 nm. Further average power scaling is straightforward by increasing the repetition rate of the pump system. As shown in Fig. 4 (a), MOPA A can deliver the necessary pulse energy for maximum spectral broadening (1.1 μJ) up to repetition rates of more than 15 MHz, enabling total SC power in the order of 10 W.

The high degree of spectral flatness of the generated SC is unprecedented in this wavelength region. Combined with the high average output power and minimal mid-IR power fluctuations of less than 0.5 dB over a 30 minute interval the system enables broadband mid-IR spectroscopic measurements with uniform spectral sensitivity and high signal-to-noise ratios in wavelength regions where various hydrocarbons, hydrochlorides and commonly used solvents display strong absorption features. This will exemplary be shown in the following section.

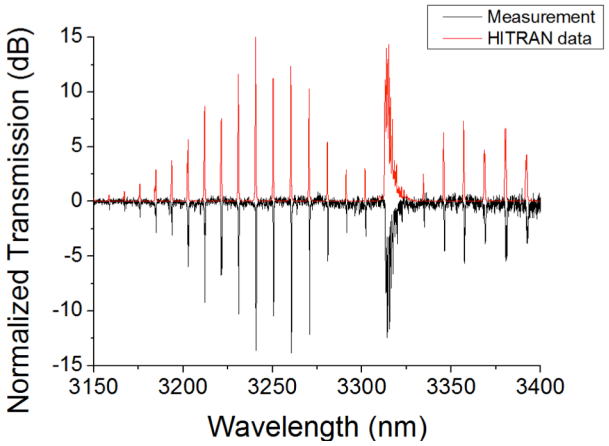

Fig. 11. Broadband, high quality mid-IR methane detection using the mid-IR SCG source from IV.B and the HC-PBGF from Fig. 10. The figure shows a high resolution (0.2 nm) transmission spectrum (black, baseline subtracted) recorded through 1.25 m HC-PBGF filled with a mixture of 1000 ppm methane in nitrogen. The absorption spectrum from the HITRAN database (red) is shown for comparison (mirrored on the baseline for clarity).

C. Mid-IR gas detection in hollow-core fibers

One of the main attractions of the mid-IR spectral region is the large number of molecules that undergo strong characteristic vibrational transitions in this domain and that can therefore be fingerprinted using their unique absorption signatures [7]. The highly sensitive detection of mid-IR absorption peaks is therefore expected to enable many local and remote sensing applications in environmental control, security, and healthcare industries. For instance, gases such as methane, ethane, and acetylene exhibit strong fundamental absorption peaks in the region between 3 – 4 μm and have been identified as biomarkers in breath analysis [70]. This non-invasive health screening technique aims to identify and quantify volatile components in human breath, which provide key information about physiological processes and enable early-detection of diseases such as renal failure, cystic fibrosis and cancer [71, 72]. However, low concentrations of multiple elements need to be detected simultaneously, which requires sensitive and broadband detection methods.

HC-PBGFs offer an excellent platform to observe weak gas-light interactions due to their tight modal confinement in the hollow core combined with their low-loss guidance. Filled with the gas under test, the hollow core fiber geometry allows extremely long interaction lengths and therefore the probing of weak gas absorption lines and low concentrations that would otherwise be difficult to observe using bulk approaches [49]. In addition, HC-PBGFs are particularly suitable for achieving small device footprints due to their low sensitivity to macro-bending such that tight coils can be formed with virtually no loss penalty [73]. Note that other air-guiding fiber geometries including hollow waveguides, anti-resonant fiber, and Kagome fibers exhibit substantially higher bend loss [74]. This is a critical issue for the design of practical sensing devices where long path lengths combined with small device form factors are required.

Most gas detection measurements in hollow core fibers to date have used the first overtone absorption lines in the near-IR [75-77], but the recent development of silica-based HC-PBGF with low loss over wide bandwidths in the mid-IR enables measurements on the much stronger fundamental absorption peaks [78, 79], which should increase sensitivity and specificity of the detection. The HC-PBGF with the lowest attenuation at mid-IR wavelengths reported to date was recently fabricated in-house and extensively characterized in [80]. Fig. 10 shows transmission and loss measurements of this fiber with (a) high dynamic range and (b) high resolution, both of which were enabled by using the SCG source described in the previous section. The measurement over a 5 m fiber length (purple line in Fig. 10(a)) shows that the bandgap extends from 3.1 to 3.8 μm and a cutback loss measurement (58 to 5 m) records a minimum loss of 0.13 (±0.05) dB/m at 3.33 μm and <1 dB/m transmission loss over a >500 nm window, which overlaps well with one of the regions of interest for gas sensing, as mentioned above. In fact, many of the oscillatory features in the loss measurement can be attributed to HCl gas absorption lines, which are present in the fiber due to the use of chlorine to dehydrate the bulk silica glass used as raw material in fabrication (Fig. 10(b)). When removed by purging the fiber with argon gas, the fiber attenuation decreases to 0.05 (±0.03) dB/m. These are particularly impressive numbers when compared to the bulk attenuation of silica, which is 100 – 600 dB/m in this spectral region [81], indicating an overlap of the guided mode with the silica cladding of only about 0.1%.

It appears that combining the powerful, flat, and stable mid-IR SCG source described in section IV.B with these low-loss guiding HC-PBGFs results in a sensitive broadband spectroscopic measurement device for gas detection in the mid-IR spectral region, as evident from the high dynamic range of the loss measurements and the high-resolution detection of the HCl absorption peaks. However, most of the HCl absorption peaks are saturated in this measurement due to the long fiber lengths used in the loss measurement.

In order to further demonstrate the capabilities of this system, we filled a 1.25 m length of the HC-PBGF with a mixture of 1000 ppm methane in nitrogen and recorded a high-resolution (0.2 nm) transmission spectrum over a broadband span of 250 nm from 3150 – 3400 nm using an optical spectrum analyzer (Yokogawa). In Fig. 11, the measurement with subtracted baseline is compared with the absorption spectrum from the HITRAN database, appropriately scaled to reflect interaction length, concentration and resolution of the measurement. The quality of the measurement and the agreement with theory is astonishing. Almost 15 dB OSNR could be achieved at the strongest absorption lines, and even the weaker lines could be resolved. In order to fully appreciate these results, they should be compared to earlier work in the mid-IR where only about 3 dB OSNR was obtained for the same methane concentration over a similar length of fiber and at a much lower resolution of 3 – 4 nm [79]. A minimum detection limit of 50 ppm was claimed in this work, which would clearly be much lower in our system. More than sufficient power was transmitted through the fiber such that detection of even lower concentrations over longer fiber lengths is certainly feasible.

While more work has to be done in order to establish the minimum detectable concentrations and perform quantitative measurements (in preparation), these initial results demonstrate a substantial qualitative increase in both OSNR and resolution of the detected absorption lines compared to previous results. Consequently, the presented system consisting of our 2 μm diode-seeded MOPA pump systems followed by a mid-IR SCG stage and a detection stage in low-loss HC-PBGF is certainly a promising approach for the realization of compact and versatile multi-band, multi-element spectroscopic measurement devices in the mid-IR for environmental, security, and healthcare applications.

V. Conclusion

Diode-seeded TDFA systems arguably offer the most practical and flexible approach currently available to generate high power pulsed laser radiation in the 2 μm wavelength region. Their capability to deliver pulses with vastly different parameters and shapes from the same laser system via straightforward electronic control is unmatched. From an applications point of view, this versatility of the laser system combined with the high stability of the pulse generation and amplification process are often more important than headline record power figures. All-fiber integration is also easy to envisage and would result in the robustness needed for commercial applications.

While we did not use very-large-mode-area fibers in order to keep the system as simple and compact as possible, large-pitch rod-type PCF fibers used in recent nanosecond work could easily be incorporated in our system and would substantially increase the observed nonlinear thresholds and enable further energy and peak-power scaling. Nonlinear pulse compression should also allow yet shorter pulses and higher peak powers.

Especially in conjunction with novel waveguide designs, such as highly nonlinear soft glass fibers or low-loss hollow core fibers, diode-seeded TDFAs are already enabling promising new research and technology pathways in the emerging waveband of 2 μm and beyond with substantial scientific and industrial impact.

Acknowledgment

The authors would like to gratefully thank Shaif-Ul Alam, Marco Petrovich, Natalie Wheeler, Jonathan Price, Yongmin Jung and Francesco Poletti for stimulating discussions and for providing some of the figures. We acknowledge OFS Denmark, Nufern, Eblana Photonics and Yokogawa for providing core and cladding pumped thulium doped fiber, laser diodes and the extended wavelength OSA, respectively.

REFERENCES

[1] D. Richardson, J. Nilsson, and W. Clarkson, "High power fiber lasers: current status and future perspectives [Invited]," *J. Opt. Soc. Am. B,* vol. 27, pp. B63-B92, 2010.

[2] C. Jauregui, J. Limpert, and A. Tünnermann, "High-power fibre lasers," *Nat. Photonics,* vol. 7, pp. 861-867, 2013.

[3] S. D. Jackson, "Towards high-power mid-infrared emission from a fibre laser," *Nat. Photonics,* vol. 6, pp. 423-431, 2012.

[4] C. Gaida, M. Gebhardt, P. Kadwani, L. Leick, J. Broeng, L. Shah, and M. Richardson, "Amplification of nanosecond pulses to megawatt peak power levels in Tm3+ -doped photonic crystal fiber rod," *Opt. Lett.,* vol. 38, pp. 691-693, 2013.

[5] P. Wan, L.-M. Yang, and J. Liu, "High pulse energy 2 μm femtosecond fiber laser," *Opt. Express,* vol. 21, pp. 1798-1803, 2013.

[6] C. Phillips, C. Langrock, J. Pelc, M. Fejer, J. Jiang, M. E. Fermann, and I. Hartl, "Supercontinuum generation in quasi-phase-matched LiNbO_3 waveguide pumped by a Tm-doped fiber laser system," *Opt. Lett.,* vol. 36, p. 3912, 2011.

[7] A. Schliesser, N. Picqué, and T. W. Hänsch, "Mid-infrared frequency combs," *Nat. Photonics,* vol. 6, pp. 440-449, 2012.

[8] N. Leindecker, A. Marandi, R. L. Byer, K. L. Vodopyanov, J. Jiang, I. Hartl, M. Fermann, and P. G. Schunemann, "Octave-spanning ultrafast OPO with 2.6-6.1 μm instantaneous bandwidth pumped by femtosecond Tm-fiber laser," *Opt. Express,* vol. 20, pp. 7046-7053, 2012.

[9] N. M. Fried and K. E. Murray, "New technologies in endourology: High-power thulium fiber laser ablation of urinary tissues at 1.94 μm," *J. Endourology,* vol. 19, pp. 25-31, 2005.

[10] F. Silva, P. Bates, A. Esteban-Martin, M. Ebrahim-Zadeh, and J. Biegert, "High-average-power, carrier-envelope phase-stable, few-cycle pulses at 2.1 μm from a collinear BiB3O6 optical parametric amplifier," *Opt. Lett.,* vol. 37, pp. 933-935, 2012.

[11] F. Stutzki, F. Jansen, C. Jauregui, J. Limpert, and A. Tünnermann, "2.4 mJ, 33 W Q-switched Tm-doped fiber laser with near diffraction-limited beam quality," *Opt. Lett.,* vol. 38, pp. 97-99, 2013.

[12] P. Wan, L.-M. Yang, and J. Liu, "156 micro-J ultrafast Thulium-doped fiber laser," *SPIE LASE,* pp. 860138-860138-7, 2013.

[13] P. Hübner, C. Kieleck, S. D. Jackson, and M. Eichhorn, "High-power actively mode-locked sub-nanosecond Tm3+ -doped silica fiber laser," *Opt. Lett.,* vol. 36, pp. 2483-2485, 2011.

[14] J. Liu, Q. Wang, and P. Wang, "High average power picosecond pulse generation from a thulium-doped all-fiber MOPA system," *Opt. Express,* vol. 20, pp. 22442-22447, 2012.

[15] P. Dupriez, A. Piper, A. Malinowski, J. Sahu, M. Ibsen, B. Thomsen, Y. Jeong, L. Hickey, M. Zervas, and J. Nilsson, "High average power, high repetition rate, picosecond pulsed fiber master oscillator power amplifier source seeded by a gain-switched laser diode at 1060 nm," *IEEE Phot. Technol. Lett.,* vol. 18, pp. 1013-1015, 2006.

[16] K. K. Chen, J. H. Price, S.-u. Alam, J. R. Hayes, D. Lin, A. Malinowski, and D. J. Richardson, "Polarisation maintaining 100W Yb-fiber MOPA producing μJ pulses tunable in duration from 1 to 21 ps," *Opt. Express,* vol. 18, pp. 14385-14394, 2010.

[17] S. Kanzelmeyer, H. Sayinc, T. Theeg, M. Frede, J. Neumann, and D. Kracht, "All-fiber based amplification of 40 ps pulses from a gain-switched laser diode," *Opt. Express,* vol. 19, pp. 1854-1859, 2011.

[18] P. S. Teh, R. J. Lewis, S.-u. Alam, and D. J. Richardson, "200 W Diffraction limited, single-polarization, all-fiber picosecond MOPA," *Opt. Express,* vol. 21, pp. 25883-25889, 2013.

[19] D. N. Schimpf, C. Ruchert, D. Nodop, J. Limpert, A. Tünnermann, and F. Salin, "Compensation of pulse-distortion in saturated laser amplifiers," *Opt. Express,* vol. 16, pp. 17637-17646, 2008.

[20] A. Malinowski, P. Gorman, C. Codemard, F. Ghiringhelli, A. Boyland, A. Marshall, M. Zervas, and M. Durkin, "High-peak-power, high-energy, high-average-power pulsed fiber laser system with versatile pulse duration and shape," *Opt. Lett.,* vol. 38, pp. 4686-4689, 2013.

[21] R. Phelan, J. O'Carroll, D. Byrne, C. Herbert, J. Somers, and B. Kelly, "Ino. 75Ga0. 25As/InP Multiple Quantum-Well Discrete-Mode Laser Diode Emitting at 2 μm," *IEEE Phot. Technol. Lett.,* vol. 24, p. 652, 2012.

[22] Z. Li, A. M. Heidt, J. M. O. Daniel, Y. Jung, S. U. Alam, and D. J. Richardson, "Thulium-doped fiber amplifier for optical communications at 2 μm," *Opt. Express,* vol. 21, pp. 9289-9297, 2013

[23] Z. Li, A. M. Heidt, N. Simakov, Y. Jung, J. M. O. Daniel, S. U. Alam, and D. J. Richardson, "Diode-pumped wideband thulium-doped fiber amplifiers for optical communications in the 1800–2050 nm window," *Opt. Express,* vol. 21, pp. 26450-26455, 2013.

[24] A. M. Heidt, Z. Li, J. Sahu, P. C. Shardlow, M. Becker, M. Rothhardt, M. Ibsen, R. Phelan, B. Kelly, S. U. Alam, and D. J. Richardson, "100 kW peak power picosecond thulium-doped fiber amplifier system seeded by a gain-switched diode laser at 2 μm," *Opt. Lett.,* vol. 38, pp. 1615-1617, 2013.

[25] Z. Li, S. U. Alam, Y. Jung, A. M. Heidt, and D. J. Richardson, "All-fiber, ultra-wideband tunable laser at 2 μm," *Opt. Lett.,* vol. 38, pp. 4739-4742, 2013.

[26] P. Paulus, R. Langenhorst, and D. Jager, "Generation and optimum control of picosecond optical pulses from gain-switched semiconductor lasers," *IEEE J. Quantum Electron.,* vol. 24, pp. 1519-1523, 1988.

[27] J. AuYeung, "Picosecond optical pulse generation at gigahertz rates by direct modulation of a semiconductor laser," *Appl. Phys. Lett.,* vol. 38, pp. 308-310, 1981.

[28] G. P. Agrawal, *Nonlinear fiber optics*: Springer, 2000.

[29] P. Anandarajah, R. Maher, Y. Xu, S. Latkowski, J. O'Carroll, S. Murdoch, R. Phelan, J. O'Gorman, and L. Barry, "Generation of coherent multicarrier signals by gain switching of discrete mode lasers," *IEEE Photonics Journal,* vol. 3, pp. 112-122, 2011.

[30] J. M. Dudley, G. Genty, and S. Coen, "Supercontinuum generation in photonic crystal fiber," *Rev. Mod. Phys.,* vol. 78, p. 1135, 2006.

[31] Z. Li, A. M. Heidt, P. S. Teh, M. Berendt, R. Phelan, B. Kelly, S. U. Alam, and D. J. Richardson, "High energy diode-seeded nanosecond 2 μm fiber MOPA systems incorporating active pulse shaping," (in preparation).

[32] L. M. Frantz and J. S. Nodvik, "Theory of pulse propagation in a laser amplifier," *J. Appl. Phys.,* vol. 34, pp. 2346-2349, 1963.

[33] R. Paschotta, J. Nilsson, A. C. Tropper, and D. C. Hanna, "Ytterbium-doped fiber amplifiers," *IEEE J. Quantum Electron.,* vol. 33, pp. 1049-1056, 1997.

[34] A. Malinowski, K. T. Vu, K. K. Chen, J. Nilsson, Y. Jeong, S. Alam, D. Lin, and D. J. Richardson, "High power pulsed fiber MOPA system incorporating electro-optic modulator based adaptive pulse shaping," *Opt. Express,* vol. 17, pp. 20927-20937, 2009.

[35] G. Sobon, P. Kaczmarek, A. Antonczak, J. Sotor, A. Waz, and K. Abramski, "Pulsed dual-stage fiber MOPA source operating at 1550 nm with arbitrarily shaped output pulses," *Appl. Phys. B,* vol. 105, pp. 721-727, 2011.

[36] P. Winzer, "Beyond 100G ethernet," *IEEE Commun. Mag.,* vol. 48, pp. 26-30, 2010.

[37] A. D. Ellis, J. Zhao, and D. Cotter, "Approaching the non-linear Shannon limit," *J. Lightwave Technol.,* vol. 28, pp. 423-433, 2010.

[38] D. J. Richardson, "Filling the light pipe," *Science,* vol. 330, pp. 327-328, 2010.

[39] E. Desurvire, C. Kazmierski, F. Lelarge, X. Marcadet, A. Scavennec, F. Kish, D. Welch, R. Nagarajan, C. Joyner, and R. Schneider Jr, "Science and technology challenges in XXIst century optical communications," *Comp. Ren. Phys.,* vol. 12, pp. 387-416, 2011.

[40] D. Richardson, J. Fini, and L. Nelson, "Space-division multiplexing in optical fibres," *Nat. Photonics,* vol. 7, pp. 354-362, 2013.

[41] F. Poletti, N. Wheeler, M. Petrovich, N. Baddela, E. N. Fokoua, J. Hayes, D. Gray, Z. Li, R. Slavík, and D. Richardson, "Towards high-capacity fibre-optic communications at the speed of light in vacuum," *Nat. Photonics,* 2013.

[42] T. Morioka, Y. Awaji, R. Ryf, P. Winzer, D. Richardson, and F. Poletti, "Enhancing optical communications with brand new fibers," *IEEE Commun. Mag.,* vol. 50, pp. s31-s42, 2012.

[43] R. Cregan, B. Mangan, J. Knight, T. Birks, P. S. J. Russell, P. Roberts, and D. Allan, "Single-mode photonic band gap guidance of light in air," *Science,* vol. 285, pp. 1537-1539, 1999.

[44] P. Roberts, F. Couny, H. Sabert, B. Mangan, D. Williams, L. Farr, M. Mason, A. Tomlinson, T. Birks, and J. Knight, "Ultimate low loss of hollow-core photonic crystal fibres," *Opt. Express,* vol. 13, pp. 236-244, 2005.

[45] J. Lyngsø, B. Mangan, C. Jakobsen, and P. Roberts, "7-cell core hollow-core photonic crystal fibers with low loss in the spectral region around 2 μm," *Opt. Express,* vol. 17, pp. 23468-23473, 2009.

[46] M. N. Petrovich, F. Poletti, J. P. Wooler, A. M. Heidt, N. K. Baddela, Z. Li, D. R. Gray, R. Slavík, F. Parmigiani, N. V. Wheeler, J. R. Hayes, E. Numkam Fokoua, L. Grüner-Nielsen, B. Pálsdóttir, R. Phelan, B. Kelly, M. Becker, N. MacSuibhne, J. Zhao, F. C. Garcia Gunning, A. Ellis, P. Petropoulos, S. U. Alam, and D. J. Richardson, "First demonstration of 2μm data transmission in a low-loss hollow core photonic bandgap fiber," in *European Conference and Exhibition on Optical Communication*, 2012.

[47] M. N. Petrovich, F. Poletti, J. P. Wooler, A. M. Heidt, N. K. Baddela, Z. Li, D. R. Gray, R. Slavík, F. Parmigiani, N. V. Wheeler, J. R. Hayes, E. Numkam Fokoua, L. Grüner-Nielsen, B. Pálsdóttir, R. Phelan, B. Kelly, M. Becker, N. MacSuibhne, J. Zhao, F. C. Garcia Gunning, A. Ellis, P. Petropoulos, S. U. Alam, and D. J. Richardson, "Demonstration of amplified data transmission at 2 μm in a low-loss wide bandwidth hollow core photonic bandgap fiber," *Opt. Express,* vol. 21, pp. 28559-28569, 2013.

[48] N. Mac Suibhne, Z. Li, B. Baeuerle, J. Zhao, J. P. Wooler, S. U. Alam, F. Poletti, M. N. Petrovich, A. M. Heidt, N. V. Wheeler, N. Baddela, E. N. Fokoua, I. Giles, D. Giles, R. Phelan, J. O'Carroll, B. Kelly, B. Corbett, D. Murphy, A. D. Ellis, D. J. Richardson, and F. G. Gunning, "WDM Transmission at 2μm over Low-Loss Hollow Core Photonic Bandgap Fiber," in *Optical Fiber Communication Conference*, 2013.

[49] F. Poletti, M. N. Petrovich, and D. J. Richardson, "Hollow-core photonic bandgap fibers: technology and applications," *Nanophotonics,* vol. 2, pp. 315-340, 2013.

[50] V. A. Sleiffer, Y. Jung, P. Leoni, M. Kuschnerov, N. Wheeler, N. Baddela, R. van Uden, C. Okonkwo, J. R. Hayes, and J. Wooler, "30.7 Tb/s (96x320 Gb/s) DP-32QAM transmission over 19-cell Photonic Band Gap Fiber," in *Optical Fiber Communication Conference*, 2013.

[51] Y. Jung, V. Sleiffer, N. Baddela, M. Petrovich, J. R. Hayes, N. Wheeler, D. Gray, E. R. Numkam Fokoua, J. Wooler, and N. Wong, "First Demonstration of a Broadband 37-cell Hollow Core Photonic Bandgap Fiber and Its Application to High Capacity Mode Division Multiplexing," in *Optical Fiber Communication Conference*, 2013.

[52] R. Thapa, K. Knabe, K. Corwin, and B. Washburn, "Arc fusion splicing of hollow-core photonic bandgap fibers for gas-filled fiber cells," *Opt. Express,* vol. 14, pp. 9576-9583, 2006.

[53] J. Wooler, D. Gray, F. Poletti, M. Petrovich, N. Wheeler, F. Parmigiani, and D. J. Richardson, "Robust Low Loss Splicing of Hollow Core Photonic Bandgap Fiber to Itself," in *Optical Fiber Communication Conference*, 2013.

[54] J. H. Price, X. Feng, A. M. Heidt, G. Brambilla, P. Horak, F. Poletti, G. Ponzo, P. Petropoulos, M. Petrovich, J. Shi, M. Ibsen, W. H. Loh, H. N. Rutt, and D. J. Richardson, "Supercontinuum generation in non-silica fibers," *Opt. Fiber Technol.,* vol. 18, pp. 327-344, 2012.

[55] V. V. Alexander, O. P. Kulkarni, M. Kumar, C. Xia, M. N. Islam, F. L. Terry Jr, M. J. Welsh, K. Ke, M. J. Freeman, M. Neelakandan, and A. Chan, "Modulation instability initiated high power all-fiber supercontinuum lasers and their applications," *Opt. Fiber Technol.,* vol. 18, pp. 349-374, 2012.

[56] C. Xia, M. Kumar, O. P. Kulkarni, M. N. Islam, F. L. Terry Jr, M. J. Freeman, M. Poulain, and G. Mazé, "Mid-infrared supercontinuum generation to 4.5 μm in ZBLAN fluoride fibers by nanosecond diode pumping," *Opt. Lett.,* vol. 31, pp. 2553-2555, 2006.

[57] G. Qin, X. Yan, C. Kito, M. Liao, C. Chaudhari, T. Suzuki, and Y. Ohishi, "Ultrabroadband supercontinuum generation from ultraviolet to 6.28 μm in a fluoride fiber," *Appl. Phys. Lett.,* vol. 95, p. 161103, 2009.

[58] C. L. Hagen, J. W. Walewski, and S. T. Sanders, "Generation of a continuum extending to the mid-infrared by pumping ZBLAN fiber with an ultrafast 1550-nm source," *IEEE Phot. Technol. Lett.,* vol. 18, pp. 91-93, 2006.

[59] C. Agger, C. Petersen, S. Dupont, H. Steffensen, J. K. Lyngsø, C. L. Thomsen, J. Thøgersen, S. R. Keiding, and O. Bang, "Supercontinuum generation in ZBLAN fibers—detailed comparison between measurement and simulation," *J. Opt. Soc. Am. B,* vol. 29, pp. 635-645, 2012.

[60] M. Eckerle, C. Kieleck, J. widerski, S. D. Jackson, G. Mazé, and M. Eichhorn, "Actively Q-switched and mode-locked Tm^{3+}-doped silicate 2μm fiber laser for supercontinuum generation in fluoride fiber," *Opt. Lett.,* vol. 37, pp. 512-514, 02/15 2012.

[61] C. Xia, Z. Xu, M. N. Islam, F. Terry, M. J. Freeman, A. Zakel, and J. Mauricio, "10.5 W Time-Averaged Power Mid-IR Supercontinuum Generation Extending Beyond 4 μm," *IEEE J. Sel. Top. Quantum Electron.,* vol. 15, pp. 422-434, 2009.

[62] W. Yang, B. Zhang, K. Yin, X. Zhou, and J. Hou, "High power all fiber mid-IR supercontinuum generation in a ZBLAN fiber pumped by a 2 μm MOPA system," *Opt. Express,* vol. 21, pp. 19732-19742, 2013.

[63] T. Schreiber, J. Limpert, H. Zellmer, A. Tünnermann, and K. P. Hansen, "High average power supercontinuum generation in photonic crystal fibers," *Opt. Commun.,* vol. 228, pp. 71-78, 12/1/ 2003.

[64] H. Chen, S. Chen, J. Wang, Z. Chen, and J. Hou, "35W high power all fiber supercontinuum generation in PCF with picosecond MOPA laser," *Opt. Commun.,* vol. 284, pp. 5484-5487, 2011.

[65] K. K. Chen, S.-U. Alam, J. H. Price, J. R. Hayes, D. Lin, A. Malinowski, C. Codemard, D. Ghosh, M. Pal, S. K. Bhadra, and D. J. Richardson, "Picosecond fiber MOPA pumped supercontinuum source with 39 W output power," *Opt. Express,* vol. 18, p. 5426, 2010.

[66] M. Kumar, C. Xia, X. Ma, V. V. Alexander, M. N. Islam, F. L. Terry, C. C. Aleksoff, A. Klooster, and D. Davidson, "Power adjustable visible supercontinuum generation using amplified nanosecond gain-switched laser diode," *Opt. Express,* vol. 16, pp. 6194-6201, 2008.

[67] O. P. Kulkarni, V. V. Alexander, M. Kumar, M. J. Freeman, M. N. Islam, F. L. Terry Jr, M. Neelakandan, and A. Chan, "Supercontinuum generation from ~1.9 to 4.5 μm in ZBLAN fiber with high average power generation beyond 3.8 μm using a thulium-doped fiber amplifier," *J. Opt. Soc. Am. B,* vol. 28, pp. 2486-2498, 2011.

[68] J. Swiderski, M. Michalska, and G. Maze, "Mid-IR supercontinuum generation in a ZBLAN fiber pumped by a gain-switched mode-locked Tm-doped fiber laser and amplifier system," *Opt. Express,* vol. 21, pp. 7851-7857, 2013.

[69] A. M. Heidt, J. H. V. Price, C. Baskiotis, J. S. Feehan, Z. Li, S. U. Alam, and D. J. Richardson, "Mid-infrared ZBLAN fiber supercontinuum source using picosecond diode-pumping at 2 μm," *Opt. Express,* vol. 21, pp. 24281-24287, 2013.

[70] C. Wang and P. Sahay, "Breath analysis using laser spectroscopic techniques: breath biomarkers, spectral fingerprints, and detection limits," *Sensors,* vol. 9, pp. 8230-8262, 2009.

[71] A. Manolis, "The diagnostic potential of breath analysis," *Clin. Chem.,* vol. 29, pp. 5-15, 1983.

[72] W. Miekisch, J. K. Schubert, and G. F. Noeldge-Schomburg, "Diagnostic potential of breath analysis—focus on volatile organic compounds," *Clin. Chim. Acta,* vol. 347, pp. 25-39, 2004.

[73] T. P. Hansen, J. Broeng, C. Jakobsen, G. Vienne, H. R. Simonsen, M. D. Nielsen, P. M. Skovgaard, J. R. Folkenberg, and A. Bjarklev, "Air-guiding photonic bandgap fibers: spectral properties, macrobending loss, and practical handling," *J. Lightwave Technol.,* vol. 22, p. 11, 2004.

[74] F. Benabid and P. Roberts, "Linear and nonlinear optical properties of hollow core photonic crystal fiber," *J. Mod. Opt.,* vol. 58, pp. 87-124, 2011.

[75] T. Ritari, H. Ludvigsen, J. C. Petersen, T. Sørensen, A. Bjarklev, and T. P. Hansen, "Gas sensing using air-guiding photonic bandgap fibers," in *Conference on Lasers and Electro-Optics*, 2004.

[76] F. Benabid, F. Couny, J. Knight, T. Birks, and P. S. J. Russell, "Compact, stable and efficient all-fibre gas cells using hollow-core photonic crystal fibres," *Nature,* vol. 434, pp. 488-491, 2005.

[77] A. van Brakel, C. Grivas, M. N. Petrovich, and D. J. Richardson, "Micro-channels machined in microstructured optical fibers by femtosecond laser," *Opt. Express,* vol. 15, pp. 8731-8736, 2007.

[78] L. Kornaszewski, N. Gayraud, J. M. Stone, W. MacPherson, A. George, J. Knight, D. Hand, and D. Reid, "Mid-infrared methane detection in a photonic bandgap fiber using a broadband optical parametric oscillator," *Opt. Express,* vol. 15, pp. 11219-11224, 2007.

[79] N. Gayraud, Ł. W. Kornaszewski, J. M. Stone, J. C. Knight, D. T. Reid, D. P. Hand, and W. N. MacPherson, "Mid-infrared gas sensing using a photonic bandgap fiber," *Appl. Opt.,* vol. 47, pp. 1269-1277, 2008.

[80] N. V. Wheeler, A. M. Heidt, N. K. Baddela, E. N. Fokoua, J. R. Hayes, S. R. Sandoghchi, F. Poletti, M. N. Petrovich, and D. J. Richardson, "Low Loss and Low Bend Sensitivity Mid-IR Guidance in a Hollow Core-Photonic Bandgap Fiber," *Opt. Lett.,* p. in press, 2013.

[81] O. Humbach, H. Fabian, U. Grzesik, U. Haken, and W. Heitmann, "Analysis of OH absorption bands in synthetic silica," *J. Non-Cryst. Solids,* vol. 203, pp. 19-26, 1996.

Alexander M. Heidt received the Diplom degree in physics from the University of Konstanz, Germany, in 2007 and a bi-national PhD degree in physics jointly awarded by the University of Jena, Germany, and Stellenbosch University, South Africa, in 2011.

Dr. Heidt joined the Optoelectronics Research Centre at Southampton University in 2012 and currently holds a Marie Curie Research Fellowship of the European Union, working on mid-infrared photonics. His current research interests include nonlinear fiber optics, specialty optical fibers, and high-power fiber lasers.

Zhihong Li received the B. Sc. degree in optics from National University of Defense Technology, Changsha, China, in 2008.

He joined the Optoelectronics Research Centre, University of Southampton in 2010 as a PhD student, working on developing novel fiber amplifiers for future optical communication networks.

David J. Richardson joined the Optoelectronics Research Centre (ORC) at Southampton University as a Research Fellow in May 1989 and was awarded a Royal Society University Fellowship in 1991 in recognition of his pioneering work on short pulse fiber lasers.

Professor Richardson is now Deputy Director of the ORC with responsibility for fiber and laser related research. His current research interests include amongst others: optical fiber communications, microstructured optical fibers and high-power fiber lasers.

He has published more than 1000 conference and journal papers and produced more than 20 patents. Professor Richardson was one of the co-founders of SPI Lasers Ltd, an ORC spin-off venture acquired by the Trumpf Group in 2008. He is a Fellow of the Optical Society of America, the Institute of Engineering and Technology and was made a Fellow of the Royal Academy of Engineering in 2009.